Multinuclear solid-state NMR: unveiling the local structure of defective MOF MIL-120

Zhang, Wanli; Chen, Shoushun; Terskikh, Victor V.; Lucier, Bryan E. G.; Huang, Yining

Publisher's version / Version de l'éditeur:
https://doi.org/10.1016/j.ssnmr.2022.101793
Solid State Nuclear Magnetic Resonance, 119, 2022-03-21

Multinuclear solid-state NMR: unveiling the local structure of defective MOF MIL-120

Zhang, Wanli; Chen, Shoushun; Terskikh, Victor V.; Lucier, Bryan E. G.; Huang, Yining

Publisher's version / Version de l'éditeur:
https://doi.org/10.1016/j.ssnmr.2022.101793
Solid State Nuclear Magnetic Resonance, 119, 2022-03-21

Multinuclear solid-state NMR: Unveiling the local structure of defective MOF MIL-120

Wanli Zhang[a ¶], Shoushun Chen[a ¶] , Victor V. Terskikh[b], Bryan E.G. Lucier[a] and Yining Huang[*a]

[a] *Department of Chemistry, The University of Western Ontario, London, Ontario, Canada N6A 5B7.*

[b] *Metrology, National Research Council Canada, Ottawa, Ontario, K1A 0R6, Canada.*

¶ These authors contributed equally to this work.

* Corresponding author; YH email: yhuang@uwo.ca.

Abstract

Metal-organic frameworks (MOFs) are an emerging material with many current and potential applications due to their unique properties. One critical feature is that the physical and chemical properties of MOFs are tunable. One of the methods for tuning MOFs' properties is to introduce defects by design for desired applications. Characterization of MOF defects is important, but very challenging due to the local nature and short-range ordering. In this work, we have introduced the ordered vacancies (the defects) in the form of the coordinatively unsaturated sites (CUSs) into the framework of MOF MIL-120(Al). The creation of the ordered vacancies is achieved by replacing a quarter of the BTEC (1,2,4,5-benzenetetracarboxylate) with BDC (benzene-1,4-dicarboxylate) linkers. Both parent and defective MOFs were characterized by multinuclear solid-state NMR spectroscopy. ^{1}H MAS NMR is used to characterize the hydrogen bonding in these MOFs, whereas ^{13}C CP MAS NMR confirms unambiguously that the BDC is incorporated into the framework. ^{27}Al 1D MAS NMR provides direct evidence on the creation of the coordinatively unsaturated Al sites (the defects). Furthermore, ^{27}Al 3QMAS experiments at 21.1 T allow the resolution of 1 penta-coordinated and 3 chemically inequivalent octahedral Al sites in the defective MIL-120(Al). Two of the above-mentioned octahedral Al sites are in the domain which is defect-free. The third octahedral Al site is near the defective site. This work clearly demonstrates the power of SSNMR spectroscopy for characterization of defective MOFs.

1. Introduction

Metal organic frameworks (MOFs) are a class of crystalline hybrid organic/inorganic porous materials constructed from metal cations/clusters and organic linkers [1–3]. MOFs have emerged as promising materials for many applications such as catalysis, gas separation/storage, sensing, drug delivery, energy storage due to their exceptionally large surface area, thermal stability, permeant porosity, structural diversity, modularity, functionality and designability [4].

One key feature of MOF-based materials is that their physical and chemical properties are tunable. An effective approach to tune MOF properties for desired applications is to introduce various defects into MOF frameworks. Introduction of defects to MOFs can be achieved either by rational design through a controllable fashion or by post-synthetic modification [5–10]. Among various methods of introducing defects by design, the formation of linker vacancy is of great interest as it can lead to coordinatively unsaturated sites (CUSs) which can enhance gas adsorption and act as extra catalytic site [5–11]. For example, the MOF $Ru_3(BTC)_2$ are constructed by ruthenium and benzene-1,3,5-tricarboxylate (BTC) linker. By using pyridine-3,5-dicarboxylate (PYDC), some BTC linkers are replaced by PYDC which leads to the formation of additional Ru CUS. Those defective Ru CUSs exhibit high activity in producing hydride species and catalyzing hydrogenation of olefins [12].

Characterization of defects in MOFs can be challenging. The commonly used powder X-ray diffraction method is less effective as it mainly detects long-range ordering and periodicity. The techniques often used for defecting characterization include AFM, TEM, EXAFS along with vibrational spectroscopy and other methods [5–8]. Solid-state NMR (SSNMR) spectroscopy is a powerful technique for MOF characterization [13–21]. In principle, it should be an effective method for characterizing defects as it probes local

structure and short-range ordering. However, SSNMR has not been used to its fullest potential for defect characterization of MOFs.

In this work, we used a simple approach to introduce the CUSs into the framework of MOF MIL-120(Al), $Al_4(OH)_8[C_{10}O_8H_2]$. MIL-120(Al) is an aluminum-pyromellitate MOF with 1,2,4,5-benzenetetracarboxylate (BTEC) linkers [22]. Its thermal stability and porosity lead to the applications such as adsorption of small gas molecules such as H_2, CH_4, CO_2 and noble gases as well as capture of iodine [23,24]. The creation of the CUSs in defective MIL-120(Al) is achieved by replacing a portion of the BTEC linkers by benzene-1,4-dicarboxylate (BDC) ligands as introducing BDC linkers results in the formation of five-coordinated Al CUSs. The pristine and defective MIL-120(Al) MOFs were characterized extensively by multinuclear (^{1}H, ^{13}C and ^{27}Al) SSNMR spectroscopy. We demonstrated that multinuclear SSNMR spectroscopy in combination with the DFT calculation is an effective approach for characterization of defective MOFs. Some preliminary results were mentioned very briefly in an early review article [17].

2. Experimental

All chemicals were obtained from Sigma-Aldrich and used without further purification.

As-made and dehydrated MIL-120(Al)

As-made MIL-120(Al) was synthesized using a previously described method [22]. Typically, 1.6 g of $Al(NO_3)_3 \cdot 9H_2O$ (4.25 mmol), 0.25 g of H_4BTEC (1 mmol), 1.7 mL of NaOH (4 M, 6.8 mmol), and 10 mL of H_2O were mixed into a 23 mL Teflon-lined stainless steel autoclave, then sealed, and heated at 210 °C for 24 h. The product was washed three times with deionized water and dried using vacuum filtration to obtain as-made MIL-120(Al). The as-made MIL-120(Al) sample was dehydrated under dynamic vacuum at 200 °C overnight to obtain dehydrated MIL-120(Al).

As-made and dehydrated defective MIL-120(Al)

Defective MIL-120(Al) was synthesized by replacing 30% H_4BTEC with H_2BDC in the initial reaction mixture. Briefly, 1.6 g of $Al(NO_3)_3 \cdot 9H_2O$ (4.25 mmol), 0.125 g of H_4BTEC (0.5 mmol), 0.084 g of H_2BDC (0.5 mmol), 1.7 mL of NaOH (4 M, 6.8 mmol), and 10 mL of H_2O were mixed into a 23 mL Teflon-lined stainless steel autoclave, sealed, and heated at 210 °C for 24 h. The product was washed three times with deionized water and dried using vacuum filtration to obtain as-made *defective* MIL-120(Al). The as-made defective MIL-120(Al) sample is heated under dynamic vacuum at 200 °C overnight to obtain dehydrated defective MIL-120(Al).

Powder X-ray diffraction

The powder X-ray diffraction patterns were recorded using an Inel CPS powder diffractometer operating using Cu Kα radiation (λ = 1.5406 Å). The reflections were collected at 2θ values ranging between 5 and 120° using an increment of 0.02°.

Solid state NMR experiments

^{13}C SSNMR experiments at 9.4 T were acquired using a Varian InfinityPlus wide-bore NMR spectrometer equipped with a 4 mm H/X/Y Varian/Chemagnetics probe. $^{1}H \rightarrow ^{13}C$ cross-polarization magic-angle spinning (CP MAS) spectra were recorded with proton decoupling. The proton-decoupling field was 57 kHz. The Hartmann-Hahn conditions was optimized on adamantane. The ^{1}H 90° pulse length was 4.4 μs. A contact time of 5 ms was used and the pulse delay was 3 s. The total scan number is 17,589. ^{13}C spectra were referenced to TMS using adamantane as a secondary reference: ^{13}C resonance with higher chemical shift at 38.57 ppm was used for the secondary referencing.

^{1}H and ^{27}Al SSNMR experiments were performed at a magnetic field of 21.1 T on a Bruker Avance II NMR spectrometer located at the *National Ultrahigh-Field NMR Facility for Solids* in Ottawa, Canada. All MAS spectra were acquired using a 2.5-mm H/X Bruker MAS probe at a spinning frequency of 31.25 kHz.

^{1}H MAS spectra were acquired using a modified rotor-synchronized spin-echo sequence [25]. ^{1}H 90° pulse length is 4 μs and the pulse delay is 5 s. 64 transients were collected for each spectrum. ^{1}H chemical shifts were referenced on the resonance at 1.85 ppm of adamantane (the secondary reference) relative to TMS.

^{27}Al [$\upsilon_0(^{27}Al)$ = 234.27 MHz] chemical shifts were referenced to 1.0 M $Al(NO_3)_3$ at 0.0 ppm. The one-pulse ^{27}Al MAS spectra were recorded using a short excitation pulse length of 0.20 μs, corresponding to a 18° pulse, and a recycle delay of 1 s. ^{27}Al 3QMAS method was used for higher resolution [26]. The spectra were obtained by utilization of a three-pulse, z-filter sequence [26,27]. The rf strengths of the first two hard pulses and the third soft pulse were optimized individually, and the optimized pulse lengths were 2.6, 0.90 and 10.00 μs for the three consecutive pulses. The spectra were obtained using a t_1 increment of 32 μs and a total of 256 t_1 increments. 468-600 scans were acquired with a repetition delay of 0.5 s.

$^{1}H \rightarrow {}^{27}Al$ cross-polarization experiments were conducted using an optimized contact time of 0.25 ms and a pulse delay of 5 s. ^{1}H 90° pulse length is 5 μs. The number of transient for obtaining each spectrum is 512.

Spectral Simulations. The Dmfit software package [28] was used to deconvolute the ^{1}H MAS and $^{1}H \rightarrow {}^{13}C$ CPMAS NMR spectra to obtain the areal ratios. The WSolids software [29] is used to simulate the ^{27}Al MAS spectra to extract the quadrupolar parameters.

DFT Calculations

GIPAW calculation. ^{27}Al NMR parameter calculations were carried out by using the gauge-including projector-augmented wave (GIPAW) method with pseudopotentials and plane-wave basis sets implemented in the CASTEP 19 code [30] (Academic Release CASTEP version). The generalized gradient approximation (GGA) proposed by Perdew, Burke, and Ernzerhof (PBE) was used for the exchange-correlation term [31]. The Vanderbilt-type ultrasoft pseudopotentials were generated using the "on-the-fly" method. For describing

the electronic wave functions with a plane-wave basis set, an energy cutoff of 610 eV was employed. The energy and force tolerance in the geometry convergence is 5.0×10^{-6} eV/atom and 0.01 eV/A, respectively. The geometry optimization was performed with all unit cell parameters taken from the single crystal structure of as-made MIL-120(Al) [22]. The δ_{iso} of ^{27}Al was evaluated using σ_{ref}, which is a chemical shielding reference, of 555.19 ppm calibrated by the linear regression of the calculated σ_{iso} within several well identified structures [32].

Cluster model. Ab initio calculations were conducted using the Gaussian 16 program [33]. The EFG and the magnetic shielding tensors of ^{27}Al in all the model clusters were calculated using hybrid density functional theory (DFT) at the B3LYP level of theory using the GIAO method with 6-311+G* basis sets. All model clusters were built from the coordinates of reported crystal structures and terminated with H atoms to balance the charges. When necessary, the clusters were optimized. All the calculations were performed using the facilities available on SHARCNET (www.sharcnet.ca). The reference shielding is taken from $Al(H_2O)_6^{3+}$ (σ_{Ref} = 576.4 ppm at same level [34]).

3. Results and discussion

The unique 3D structure of MIL-120(Al) is built on infinite chains of edge-sharing $Al(OH)_4O_2$ octahedra connected by 1,2,4,5-benzenetetracarboxylate (BTEC) linkers (Figure 1a and 1b). The Al ion in each AlO_6 octahedron is bound to 4 hydroxyl groups and two oxygen atoms from two BTEC linkers, and each BTEC ligand in the framework binds eight six-coordinate Al centers (Figure 1c).

The strategy for introducing the linker vacancy is simply to substitute a portion of the BTEC for BDC linker, yielding five-coordinate Al atoms in the framework as the CUSs (i.e. the defect sites). Replacing each BTEC with a single BDC ligand generates four CUSs

(Figure 1d). As mentioned above, characterization of defects in MOFs are often not very straightforward because they are localized and their distribution often irregular. Indeed, the PXRD patterns of defect-free and defective MIL-120(Al) look almost identical (Figure S1), giving no indication whether the BDC ligand is incorporated into the MIL-120(Al) framework. Thus, SSNMR experiments were performed to probe the defect sites in the framework.

^{1}H MAS NMR spectra of as-made and dehydrated MIL-120(Al) along with the defective MIL-120(Al) were acquired at 21.1 T at a spinning rate of 31.25 kHz and are shown in Figure 2. The spectrum of as-made MIL-120(Al) displays three signals, which is consistent with that reported in the literature [22]. The peak with the largest chemical shift at 7.8 ppm is due to the phenyl ring protons of the BTEC linker and the broad resonance centered at 5.0 ppm originates from the water molecules occluded inside MOF channels. The very strong signal at 3.5 ppm results from the bridging hydroxyl groups [22]. To properly analyze the relative peak intensity, the spectrum of empty rotor was acquired under identical conditions (Figure S2). The difference spectrum was obtained by subtracting the spectrum of empty rotor from the spectrum of as-made MIL-120(Al) to remove the probe background. This difference spectrum was then deconvoluted (Figure S3). The three peaks at 7.8, 5.0, 3.5 ppm have relative intensities **1:2:5.6**, compared to the predicted values of **1:4.5:4** which are derived from the unit cell content. The fact that the observed intensity ratio between CH and OH is larger than the predicted value suggests that the peak at 3.5 ppm contains the contributions from not only the bridging hydroxyl protons, but also water molecules. Thus, the proper intensity ratio between CH:H_2O:OH is **1:3.6:4**. The data suggest that measured intensity of protons from water is still smaller than the expected value and this discrepancy likely results from sample heating due to fast sample spinning at 31.25 kHz, a situation also reported in a previous study [35].

Upon dehydration, the ^{1}H MAS spectrum exhibits significant change. The peak position of phenyl ring proton remains unchanged at 7.8 ppm. The two resonances due to water and

bridging hydroxyl groups at 5.0 and 3.5 ppm in the spectrum of the as-made phase now appear at 4.2, 3.0 and 1.8 ppm. The relative intensity ratio between phenyl proton and the sum of three peaks with smaller chemical shifts is **1:3.5**, suggesting that water has been removed from the framework. Therefore, we tentatively assign all three peaks at 4.2, 3.0 and 1.8 ppm to μ_2-OH groups. Dehydration leads to the removal of hydrogen bonding of water (H1…OW1=2.04 Å) with some μ_2-OH groups (see Figure S4), leading to the protons in μ_2-OH groups free of hydrogen bonding shifting to lower chemical shift at 1.8 ppm. Dehydration is also known to promote intramolecular hydrogen bonding in MOF systems (e.g. MIL-53(Al) [36]). In the present case, removal of water likely results in the formation of hydrogen bonding between the hydroxyl groups of adjacent Al chains (H2…O1=1.91 Å) as shown in geometrically optimized structure (see Figure S4), which leads to the appearance of the peak at 4.2 ppm.

The ^{1}H MAS spectrum of as-made defective MIL-120(Al) looks like the pristine MOF (Figure 2), showing no indication whether the BDC is incorporated into the framework. This result is not entirely surprising as the ^{1}H chemical shifts of phenyl protons in BTEC and BDC in DMSO-d_6 solution are almost identical as each exhibits a single peak at 7.96 and 8.08 ppm, respectively. Deconvoluted ^{1}H spectrum reveals a small broad peak with the highest chemical shift (Figure S3). This signal might be due to OH^- as charge balancing ions in the framework [37,38].

^{13}C CP MAS NMR spectra (Figure 3), on the other hand, provide a definite answer for BDC incorporation. The spectra of both as-made and dehydrated MIL-120(Al) both contain three signals at 176, 137 and 128 ppm, which can be assigned to carboxylate, aromatic quaternary, and aromatic CH carbons, respectively [22]. For defective MIL-120(Al), in addition to the three peaks belonging to the BETC linker, two new weak resonances were also observed: one at 171 ppm along with a weak shoulder at 134 ppm on the high chemical shift side of the 128 ppm peak of the BTEC. The ^{13}C MAS spectrum of the BDC linker in MIL-53(Al) exhibits 170, 136 and 128 ppm due to carboxylate, aromatic

quaternary, and aromatic CH carbons, respectively [36,39]. Thus, we assigned the 171 and 134 ppm peaks to the BDC linker. For carboxylate and aromatic quaternary carbons, the differences in their ^{13}C chemical shifts between the BTEC and BDC linkers are large enough, allowing us to unambiguously identify the BDC incorporated inside the MIL-120(Al) framework. As mentioned above, the two peaks at 176 and 171 ppm in the carboxylate region are due to the BTEC and BDC linkers, respectively. Their relative intensities are 85.3 and 14.7 % (Figure S5), implying the ratio of the BTEC to BDC is **3:1**. This result indicates that 25% of the BTEC was replaced by BDC.

After confirming the successful substitution of a portion of BDC for BTEC, we turned our attention to characterizing the defect site itself. As mentioned earlier, introducing BDC yields five-coordinated Al centers, which are coordinatively unsaturated sites (CUSs), also known as open mental sites (OMSs). For MIL-120(Al), the ^{27}Al is an ideal nucleus for directly probing CUSs' local structure by ^{27}Al SSNMR.

Figure 4 illustrates the ^{27}Al MAS NMR spectra of pristine and defective MOF MIL-120(Al). The spectrum of as-made MIL-120(Al) contains a rather broad envelop centered in the spectral region where octahedral Al appears. Single crystal structure of MIL-120(Al) indicates that there are two inequivalent octahedral Al sites, which is consistent with the fact that the observed spectrum cannot be simulated using a single Al site. The appearance of the spectrum of dehydrated MIL-120(Al) is similar to that of as-made phase, suggesting that dehydration does not affect the Al local environments significantly. However, the ^{27}Al MAS spectrum of defective MIL-120(Al) looks drastically different from the pristine and dehydrated MIL-120(Al). It should be pointed out that partial substitution of BDC for BTEC does not change the topology of this MOF as is evidenced by that the PXRD patterns of parent and defective MOFs are very similar. However, ^{27}Al MAS NMR spectra clearly indicates marked changes in local structures of Al centers although the overall framework structure is preserved. Specifically, the spectrum of defective MOF has three spectral envelops with their centers of gravity positioned at around 25, 6 and -2 ppm. The resonance

at about 25 ppm can be unambiguously assigned to five-coordinated Al site based on its chemical shift [32]. Thus, ^{27}Al SSNMR provides direct evidence of the formation of desired CUSs. The results of PXRD, ^{13}C and ^{27}Al SSNMR confirm that the approach targeting the formation of the UCS in defective MIL-120(Al) worked as expected. The other two signals at low chemical shift are inequivalent octahedral Al sites.

1D ^{27}Al MAS spectra presented in Figure 4 have limited resolution and, therefore, exhibit broad spectral envelop(s) resulting from overlapping resonances. This is due to the facts that ^{27}Al ($I = 5/2$) is a quadrupolar nucleus and that spinning sample at magic-angle cannot completely remove line broadening originating from the second-order quadrupolar interaction. To achieve higher spectral resolution, we performed ^{27}Al MQMAS (3QMAS) experiments as MQMAS can completely eliminate the anisotropic second-order quadrupolar interaction experienced by the half-integer quadrupolar nuclei. Furthermore, since MQMAS is a 2D technique it can separate multiple sites whose signals are overlapped in 1D spectra.

In the 3QMAS spectrum of the as-made MIL-120(Al) sample (Figure 5a), the overlapping signals in the 1D MAS spectrum now is well separated into two resonances, which is consistent with the crystal structure. For each site, its quadrupolar parameters (C_Q, η_Q and δ_{iso}) were first extracted by simulating the line-shape obtained from the F2 cross-section and these values are then used as initial inputs for simulating the 1D ^{27}Al MAS spectrum. The refined final values are given in Table 1. The local environments of the two inequivalent octahedral Al centers are shown in Figure 1c [22]. The two oxygen atoms from two BTEC linkers bound to Al2 are in *trans* positions, whereas these two oxygens are *cis* to each other in the coordination sphere of Al1. To assign these two signals resolved in the 3QMAS spectrum, theoretical calculations were conducted using GIPAW approach implemented in the CASTEP code. The results obtained by using both reported single crystal structure and geometry optimized structure (Table 1) indicate that the Al2 site has a smaller isotropic chemical shift and a much larger C_Q value, whereas Al1 site has a much

small C_Q and a larger chemical shift (Table 1). Therefore, we confidently assign the resonance with the larger C_Q to Al2. The calculated C_Q values of both sites match very well with those obtained experimentally. Careful inspection of the cross section taken through Al1 site reveals a very weak signal with a large chemical shift (Figure 5). This small peak is due to a very small amount of impurity.

The overall appearance of the 3QMAS spectrum of dehydrated sample (Figure 5b) looks similar to that of the as-made phase. It also contains two Al signals with similar line-shapes to those of the Al1 and Al2 sites of the as-made sample. The narrower signal has a smaller chemical shift. Although these two sites have η_Q values close to the sites in the as-made phase, the C_Q values have changed. Specifically, the C_Q of Al1 increases from 4.9 to 6.2 MHz and the C_Q of Al2 decreases from 8.0 to 6.8 MHz upon dehydration. The difference in chemical shift between Al1 and Al2 also becomes smaller upon dehydration. As mentioned earlier, dehydration causes significant changes in hydrogen bonding and consequently the Al local environment, leading to the changes in the spectrum. We also carried out the GIPAW calculation. However, since the crystal structure of dehydrated MIL-120(Al) is unknown, we simply used the structure of the as-made MOF by removing the water molecules from the structure. But the C_Q of Al1 is underestimated, and C_Q of Al2 overestimated significantly (Table 1).

The 3QMAS spectrum of defective MOF looks markedly different from those of pristine MIL-120(Al) and displays 4 well resolved signals (Figure 5c), corresponding to 4 sites in the defective framework. Each signal exhibits a well-defined quadrupolar line-shape, implying that each Al site has rather ordered local environment. The signal (S4) due to Site 4 with the highest chemical shift is due to the five-coordinated Al. Three signals (S2-4) with lower chemical shifts originate from inequivalent octahedral Al sites (Site 2-4). A comparison with the 3QMAS spectrum of as-made MIL-120(Al) indicates that Sites 2 and 3 correspond the Al1 and Al2 in the pristine MIL-120(Al), i.e. signals 2 and 3 are due to is the Al atoms with two BTEC linkers in *cis* and *trans* positions, respectively (Figure 5 and

Table 1). This finding suggests that in the defective MOF, there are domains which are defect-free and both the long-range and short-range ordering of Al centers in these regions are similar to Al1 and Al2 in the parent MOF. The two signals with the highest (S1) and lowest (S4) chemical shifts are due to the 5- and 6-coordinated Al sites in the region that contains defects. The simple cluster modelling suggests that the 6-corrdinate Al with the lowest chemical shift is due to the octahedral Al which is bound to one BTEC and one BDC in addition to 4 μ_2-OH groups (Figure S6a). In a larger cluster model, the chemical shifts of Al sites bound to two BTEC linkers and 4 μ_2-OH groups immediately adjacent to a CUS also exhibit lower chemical shifts compared to the defect-free Al sites (Figure S6b). Either way the octahedral Al with the lowest chemical shift is very close to the defect.

To further probe the local environment of Al sites, $^{1}H \rightarrow {}^{27}Al$ CP experiments were conducted and the CP spectra are given in Figure 6. For the as-made sample, careful inspection of the spectrum reveals that the intensity of Al1 appears to be stronger than that of Al2 as a small "peak" labeled with # (which is part of the line-shape of Al2) in the one-pulse MAS spectrum disappeared. The possible reasons for this observation could be two folded. (i) The C_Q of value of Al2 is much larger than that Al1, which results in a much short $T_{1\rho}$(Al), leading to the fast decay of the CP signal. However, since the contact time used is very short, this may not be the major factor. (ii) Each Al has 4 directly attached OH groups. The Al-H distances between Al and H in the OH groups for Al1 are shorter than those for Al2 (Table S1). Furthermore, the distance between Al and the closet phenyl protons on the nearest BTEC is also shorter for Al1 than Al2 (Table S1). Similar CP behavior is also observed for dehydrated MIL-120(Al).

Defective MIL-120(Al) was also dehydrated under the same conditions as parent MIL-120(Al). However, PXRD pattern shows that dehydrated defective material is amorphous. (Figure S1) Interestingly, its ^{27}Al 1D and 2D 3QMAS, $^{1}H \rightarrow {}^{27}Al$ CP, $^{1}H \rightarrow {}^{13}C$ CP MAS and ^{1}H MAS spectra are similar to those of as-made defective MIL-120(Al), implying that the local structures around 5- and 6-corridnated Al sites as well as organic linkers are

preserved. It appears that the framework with defects is less rigid. This is because the structure of MIL-120(Al) is formed via connection of infinite zig-zag AlO_6 octahedra chains by BTEC linker. Replacing a BTEC with a BDC linker reduces the connecting points from 8 to 4, weakening the connection between the parallel chains. Consequently, the spatial arrangement of the chains lost long-range ordering after dehydration as shown in Figure 7.

4. Conclusion

The coordinatively unsaturated Al (the defective) sites were created in the framework of MOF MIL-120(Al) by substituting a quarter of BTEC with BDC linkers. Both the parent and defective MIL-120(Al) were thoroughly characterized by multinuclear SSNMR spectroscopy. ^{1}H MAS NMR was employed to obtain the information regarding the hydrogen bonding. ^{13}C CP MAS experiments were carried out to directly prove the incorporation of the BDC linker into the MIL-120(Al). ^{27}Al MAS was used to provide direct proof of the formation of the CUCs. ^{27}Al 3QMAS experiments allow us to further identify three octahedral Al sites with two of them in defect-free region and one in the domain where defects occur. SSNMR results confirm the ordered Al and linker vacancies in MOF MIL-120(Al).

Acknowledgements.

Y.H. thanks the Natural Science and Engineering Research Council (NSERC) of Canada for a Discovery Grant. Access to the 900 MHz NMR spectrometer was provided by the National Ultrahigh-Field NMR Facility for Solids (Ottawa, Canada). The National Ultrahigh-Field NMR Facility for Solids (Ottawa, Canada) is a national research facility funded by the Canada Foundation for Innovation, the Ontario Innovation Trust, Recherche Québec, the National Research Council Canada, and Bruker BioSpin and managed by the University of Ottawa.

References

[1] S. L. James, Metal-organic frameworks, *Chem. Soc. Rev.* 32(5) (2003) 276–288.

[2] S. Kitagawa, Metal–organic frameworks (MOFs), *Chem. Soc. Rev.* 43(16) (2014) 5415–5418.

[3] H.-C. Zhou, J. R. Long, O. M. Yaghi, Introduction to metal–organic frameworks, *Chem. Rev.* 112(2) (2012) 673–674.

[4] H. Furukawa, K. E. Cordova, M. O'Keeffe, O. M. Yaghi, The chemistry and applications of metal-organic frameworks, *Science.* 341(6149) (2013).

[5] D. S. Sholl, R. P. Lively, Defects in metal-organic frameworks: challenge or opportunity?, *J. Phys. Chem. Lett.* 6(17) (2015) 3437–3444.

[6] Y. Cao, X. Mi, X. Li, B. Wang, Defect engineering in metal–organic frameworks as futuristic options for purification of pollutants in an aqueous environment, *Front. Chem.* 9 (2021) 1–15.

[7] S. Dissegna, K. Epp, W. R. Heinz, G. Kieslich, R. A. Fischer, Defective metal-organic frameworks, *Adv. Mater.* 30(37) (2018).

[8] J. Ren, M. Ledwaba, N. M. Musyoka, H. W. Langmi, M. Mathe, S. Liao, W. Pang, Structural defects in metal–organic frameworks (MOFs): Formation, detection and control towards practices of interests, *Coord. Chem. Rev.* 349 (2017) 169–197.

[9] W. Xiang, Y. Zhang, Y. Chen, C. J. Liu, X. Tu, Synthesis, characterization and application of defective metal-organic frameworks: Current status and perspectives, *J. Mater. Chem. A*. 8(41) (2020) 21526–21546.

[10] Z. Fang, B. Bueken, D. E. De Vos, R. A. Fischer, Defect-engineered metal-organic frameworks, *Angew. Chemie - Int. Ed.* 54(25) (2015) 7234–7254.

[11] Y. Feng, Q. Chen, M. Jiang, J. Yao, Tailoring the properties of UiO-66 through defect engineering: A review, *Ind. Eng. Chem. Res.* 58(38) (2019) 17646–17659.

[12] W. Zhang, M. Kauer, O. Halbherr, K. Epp, P. Guo, M. I. Gonzalez, D. J. Xiao, C. Wiktor, F. X. LIabrés i Xamena, C. Wöll, Ruthenium metal-organic frameworks with different defect types: influence on porosity, sorption, and catalytic properties, *Chem. Eur. J.* 22(40) (2016) 14297–14307.

[13] V. J. Witherspoon, J. Xu, J. A. Reimer, Solid-state NMR investigations of carbon dioxide gas in metal-organic frameworks: Insights into molecular motion and adsorptive behavior, *Chem. Rev.* 118(20) (2018) 10033–10048.

[14] Y. T. A. Wong, V. Martins, B. E. G. Lucier, Y. Huang, Solid-state NMR spectroscopy: A powerful technique to directly study small gas molecules adsorbed in metal–organic frameworks, *Chem. - A Eur. J.* 25(8) (2019) 1848–1853.

[15] S. Li, O. Lafon, W. Wang, Q. Wang, X. Wang, Y. Li, J. Xu, F. Deng, Recent advances of solid-state NMR spectroscopy for microporous materials, *Adv. Mater.* 32(44) (2020) 1–22.

[16] M. Bertmer, Solid-state NMR of small molecule adsorption in metal–organic frameworks (MOFs), *Annu. Reports NMR Spectrosc.* 101 (2020) 1–64.

[17] B. E. G. Lucier, S. Chen, Y. Huang, Characterization of metal–organic frameworks: Unlocking the potential of solid-state NMR, *Acc. Chem. Res.* 51(2) (2018) 319–330.

[18] Y. Fu, H. Guan, J. Yin, X. Kong, Probing molecular motions in metal-organic frameworks with solid-state NMR, *Coord. Chem. Rev.* 427 (2021) 213563.

[19] E. Brunner, M. Rauche, Solid-state NMR spectroscopy: an advancing tool to analyse the structure and properties of metal-organic frameworks, *Chem. Sci.* 11(17) (2020) 4297–4304.

[20] A. Sutrisno, Y. Huang, Solid-state NMR: A powerful tool for characterization of metal-organic frameworks, *Solid State Nucl. Magn. Reson.* 49–50 (2013) 1–11.

[21] H. C. Hoffmann, M. Debowski, P. Müller, S. Paasch, I. Senkovska, S. Kaskel, E. Brunner, Solid-state NMR spectroscopy of metal-organic framework compounds (MOFs), *Materials.* 5(12) (2012) 2537–2572.

[22] C. Volkringer, T. Loiseau, M. Haouas, F. Taulelle, D. Popov, M. Burghammer, C. Riekel, C. Zlotea, F. Cuevas, M. Latroche, Occurrence of uncommon infinite chains consisting of edge-sharing octahedra in a porous metal organic framework-type aluminum pyromellitate $Al_4(OH)_8[C_{10}O_8H_2]$(MIL-120): Synthesis, structure, and gas sorption properties, *Chem. Mater.* 21(24) (2009) 5783–5791.

[23] S. Chibani, F. Chiter, L. Cantrel, J.-F. Paul, Capture of iodine species in MIL-53 (Al), MIL-120 (Al), and HKUST-1 (Cu) periodic DFT and ab-initio molecular dynamics studies, *J. Phys. Chem. C*. 121(45) (2017) 25283–25291.

[24] C. Falaise, C. Volkringer, J. Facqueur, T. Bousquet, L. Gasnot, T. Loiseau, Capture of iodine in highly stable metal–organic frameworks: a systematic study, *Chem. Commun.* 49(87) (2013) 10320–10322.

[25] XXXXXXXXXXXXXXXXX

[26] L. Frydman, J. S. Harwood, Isotropic spectra of half-integer quadrupolar spins from bidimensional magic-angle spinning NMR, *J. Am. Chem. Soc.* 117(19) (1995) 5367–5368.

[27] J.-P. Amoureux, C. Fernandez, S. Steuernagel, ZFiltering in MQMAS NMR, *J. Magn. Reson. A*. 123(1) (1996) 116–118.

[28] D. Massiot, F. Fayon, M. Capron, I. King, S. Le Calvé, B. Alonso, J. Durand, B. Bujoli, Z. Gan, G. Hoatson, Modelling one-and two-dimensional solid-state NMR spectra, *Magn. Reson. Chem.* 40(1) (2002) 70–76.

[29] K. Eichele, R. E. Wasylishen, WSolids1, version 1.19. 11, *Univ. Tübingen, Tübingen, Ger.* (2009).

[30] S. J. Clark, M. D. Segall, C. J. Pickard, P. J. Hasnip, M. I. J. Probert, K. Refson, M. C. Payne, First principles methods using CASTEP, *Zeitschrift für Krist. Mater.* 220(5–6) (2005) 567–570.

[31] J. P. Perdew, K. Burke, M. Ernzerhof, Generalized gradient approximation made simple, *Phys. Rev. Lett.* 77(18) (1996) 3865.

[32] M. Choi, K. Matsunaga, F. Oba, I. Tanaka, ^{27}Al NMR chemical shifts in oxide crystals: A first-principles study, *J. Phys. Chem. C*. 113(9) (2009) 3869–3873.

[33] M J Frisch et al., Gaussian 16. Gaussian, Inc. Wallingford, CT, 2016.

[34] Z. Qian, H. Feng, L. He, W. Yang, S. Bi, Assessment of the accuracy of theoretical methods for calculating 27Al nuclear magnetic resonance shielding tensors of aquated aluminum species, *J. Phys. Chem. A*. 113(17) (2009) 5138–5143.

[35] J. Brus, Heating of samples induced by fast magic-angle spinning, *Solid State Nucl. Magn. Reson.* 16(3) (2000) 151–160.

[36] T. Loiseau, C. Serre, C. Huguenard, G. Fink, F. Taulelle, M. Henry, T. Bataille, G. Férey, A rationale for the large breathing of the porous aluminum terephthalate (MIL-53) upon hydration,

Chem. Eur. J. 10(6) (2004) 1373–1382.

[37] T. Liu, Z. Liu, G. Kim, J. T. Frith, N. Garcia-Araez, C. P. Grey, Understanding LiOH chemistry in a Ruthenium-catalyzed Li–O_2 battery, *Angew. Chemie Int. Ed.* 56(50) (2017) 16057–16062.

[38] E. G. Sorte, J. M. Rimsza, T. M. Alam, Computational and experimental ^{1}H-NMR study of hydrated Mg-based minerals, *Molecules*. 25(4) (2020) 933.

[39] C. Lieder, S. Opelt, M. Dyballa, H. Henning, E. Klemm, M. Hunger, Adsorbate effect on $AlO_4(OH)_2$ centers in the metal-organic framework MIL-53 investigated by solid-state NMR spectroscopy, *J. Phys. Chem. C*. 114(39) (2010) 16596–16602.

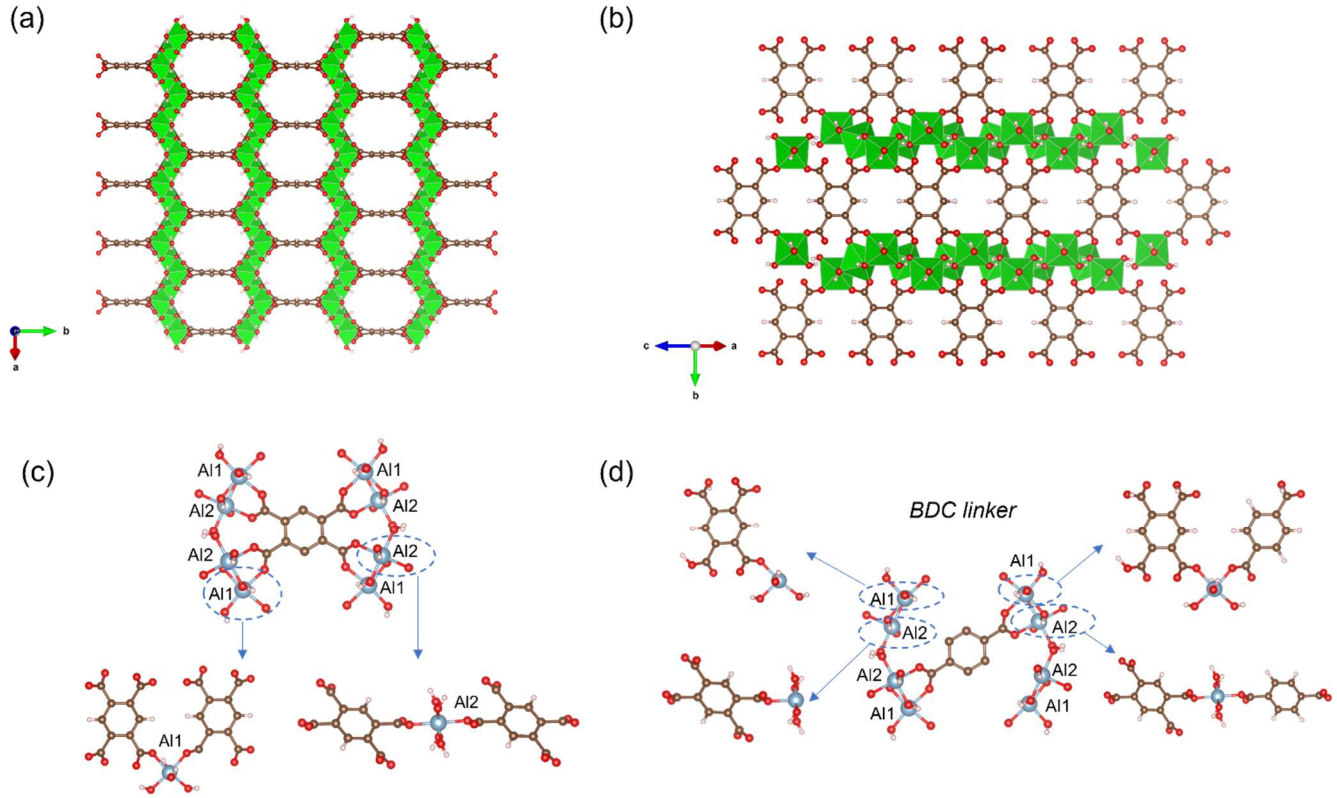

Figure 1. Structure of MIL-120(Al) viewing along (a) (001) direction and (b) (101) direction; (c) Illustration of two chemically inequivalent Al sites in MIL-120(Al) and the connectivity of the BTEC linker; (d) Illustration of the formation of defects with BDC substitution.

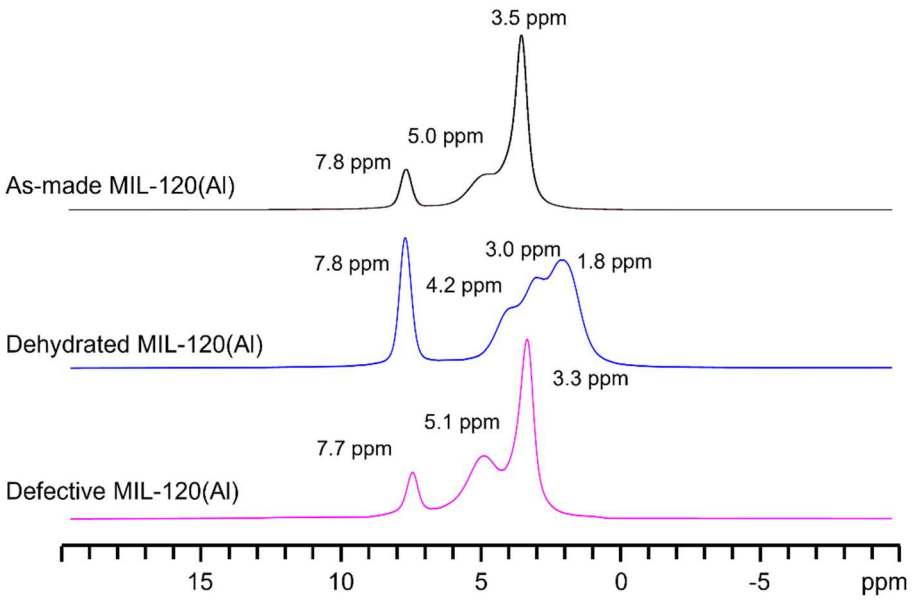

Figure 2. ^{1}H MAS NMR spectra of as-made MIL-120(Al), dehydrated MIL-120(Al) and defective MIL-120(Al).

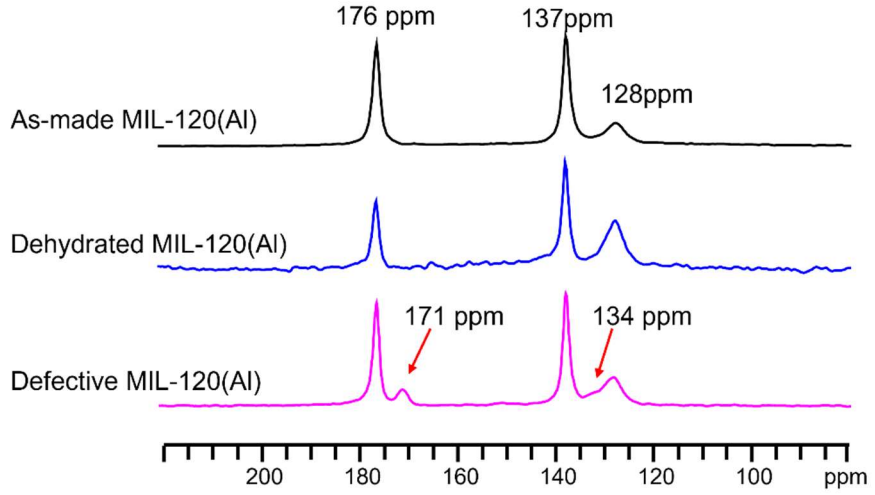

Figure 3. $^{1}H \rightarrow {}^{13}C$ CP MAS NMR spectra of as-made MIL-120(Al), dehydrated MIL-120(Al) and defective MIL-120(Al).

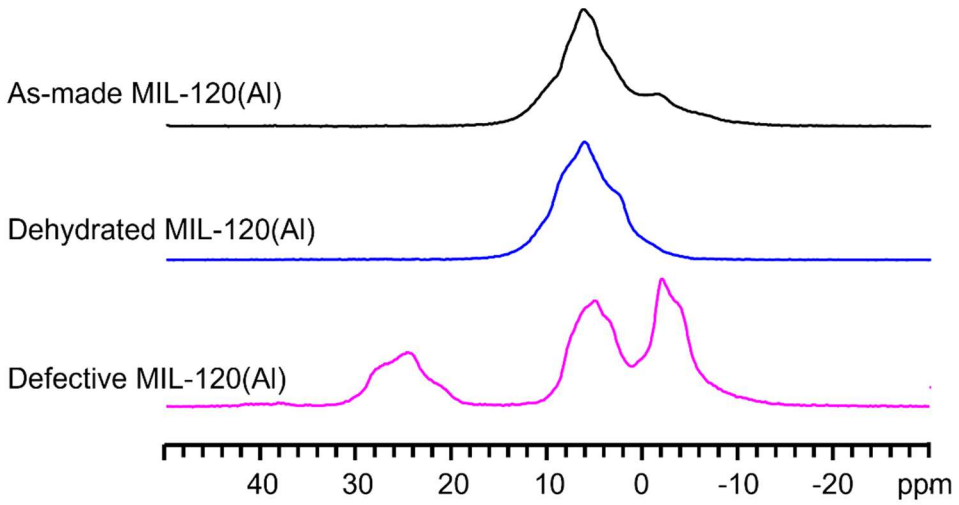

Figure 4. ^{27}Al MAS NMR spectra of as-made MIL-120(Al), dehydrated MIL-120(Al) and defective MIL-120(Al).

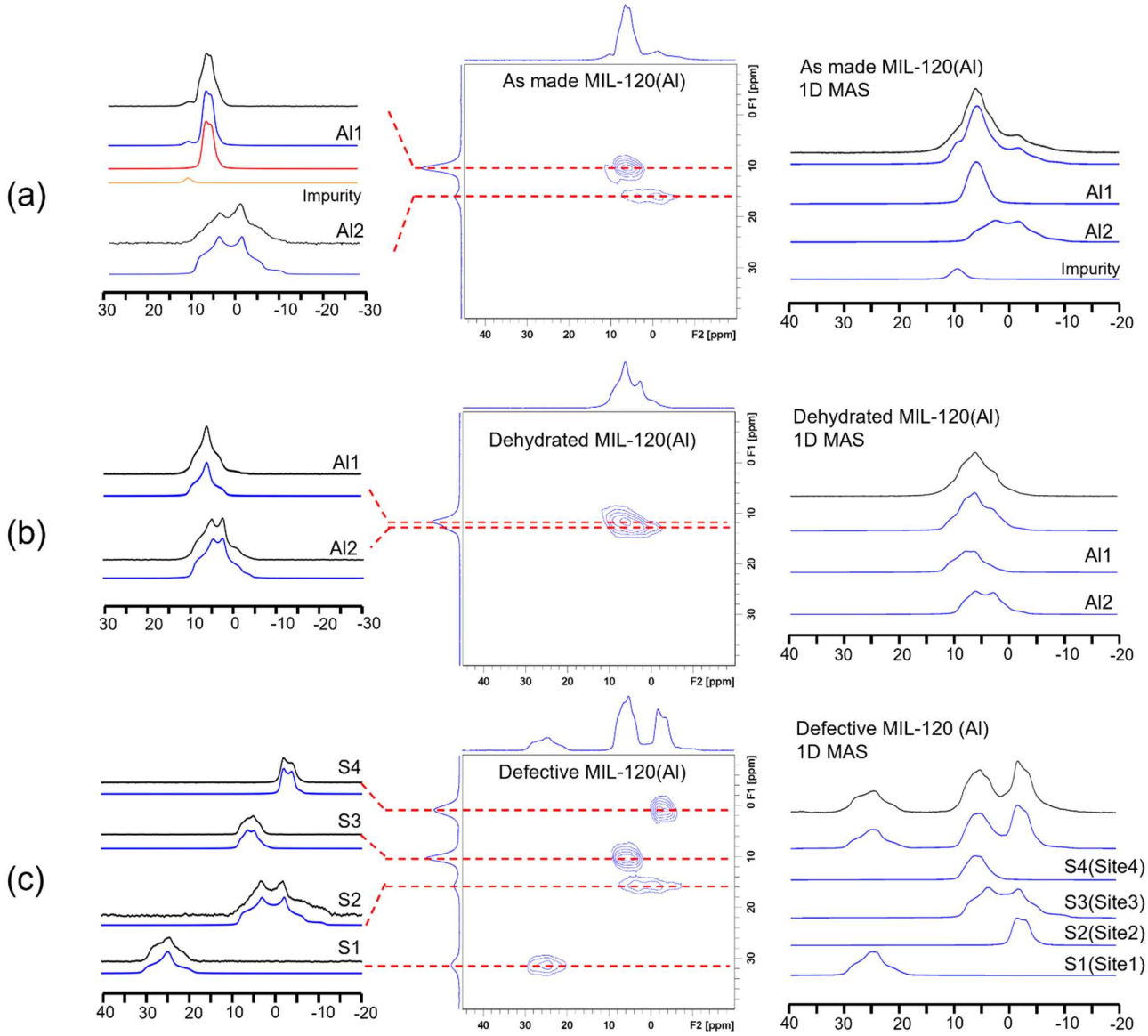

Figure 5. Left: ^{27}Al 3QMAS spectra of as-made MIL-120(Al), dehydrated MIL-120(Al) and defective MIL-120(Al). The dashed lines correspond to the slices taken along F2 cross-section. Right: The ^{27}Al MAS spectra simulated with the parameters obtained from 3QMAS data (black line: experimental, blue line: simulated).

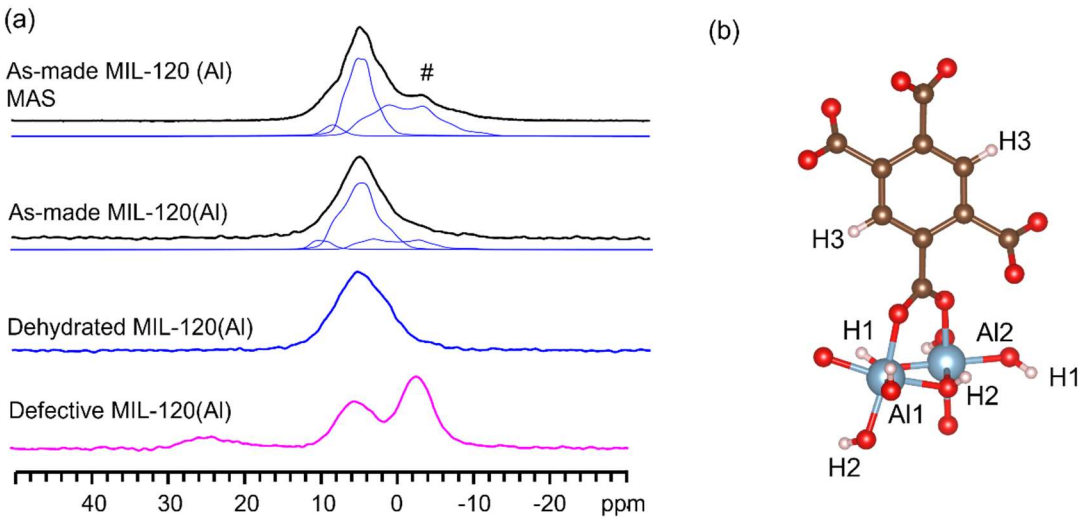

Figure 6. (a) $^{1}H \rightarrow {}^{27}Al$ CP MAS NMR spectra of as-made MIL-120(Al), dehydrated MIL-120(Al) and defective MIL-120(Al). The ^{27}Al MAS spectra of as-made MIL-120(Al) is also shown on the top for comparison. (b) Illustration of the positions of hydrogen atoms relative to Al sites.

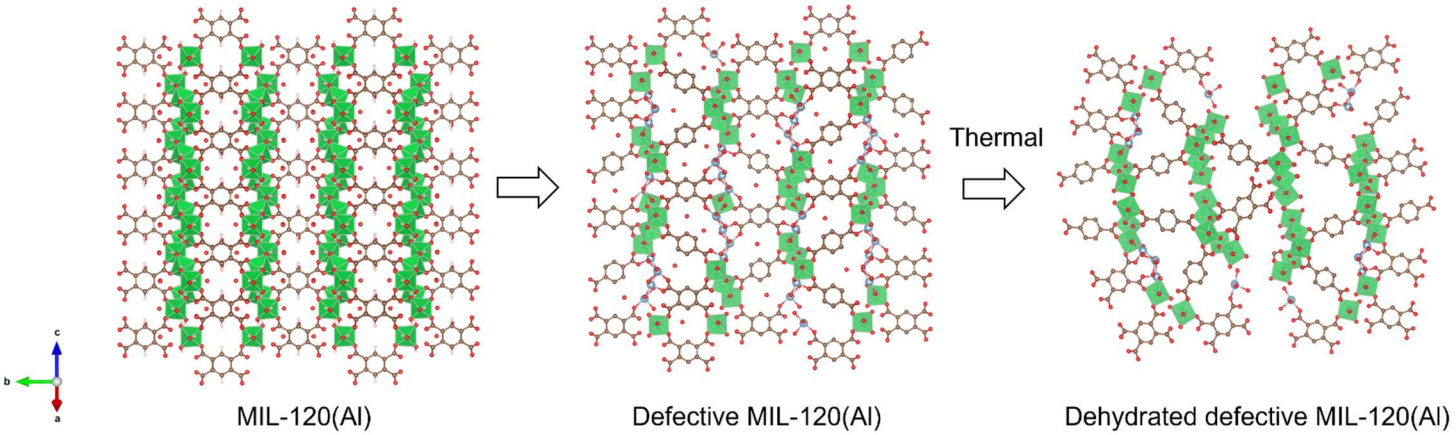

Figure 7. Schematic illustration of the defect formation and amorphization in MIL-120(Al) after dehydration

Table 1. Experimental and calculated ^{27}Al NMR parameters

	δ_{iso}(ppm)	C_Q (MHz)	η_Q
As-made MIL-120(Al)			
Experiment [a]			
Al2	7.9	8.0	0.45
Al1	9.3	4.9	0.58
Impurity	12.9	4.8	0.80
CASTEP [b]			
Al2	5.45	8.7	0.65
Al1	11.5	4.9	0.68
Dehydrated MIL-120(Al)			
Experiment [a]			
Al2	9.7	6.8	0.41
Al1	11.9	6.2	0.60
CASTEP [c]			
Al2	5.13	8.0	0.87
Al1	11.2	4.3	0.68
CASTEP [d]			
Al1	11.1	3.9	0.49
Al2	12.8	10.4	0.62
CASTEP [e]			
Al1	10.5	4.9	0.66
Al2	13.4	9.4	0.84
Defective MIL-120(Al)			
Experiment [a]			
S4 (Site 4)	-0.3	4.6	0.25
S3 (Site 3)	8.7	5.1	0.52
S2 (Site 2)	9.0	8.5	0.38

S1 (Site 1)	29.5	6.1	0.70

a. Simulation from 1D MAS. b. GIPAW calculation with geometry optimization of hydrogen atoms of water molecules. c. GIPAW calculation with crystal structure [22] after removal of water molecules. d. GIPAW calculation with (c) after geometry optimization of all atoms e. GIPAW calculation with (c) after geometry optimization of hydrogen atoms.

Supporting Information

Multinuclear solid-state NMR: Unveiling the local structure of defective MOF MIL-120

Wanli Zhang[a ¶], Shoushun Chen[a ¶] , Victor V. Terskikh[b], Bryan E.G. Lucier[a] and Yining Huang[*a]

[a] *Department of Chemistry, The University of Western Ontario, London, Ontario, Canada N6A 5B7.*

[b] *Metrology, National Research Council Canada, Ottawa, Ontario, K1A 0R6, Canada*

¶ These authors contributed equally to this work.

* Corresponding author; YH email: yhuang@uwo.ca.

Table of contents

Supporting items **Page**

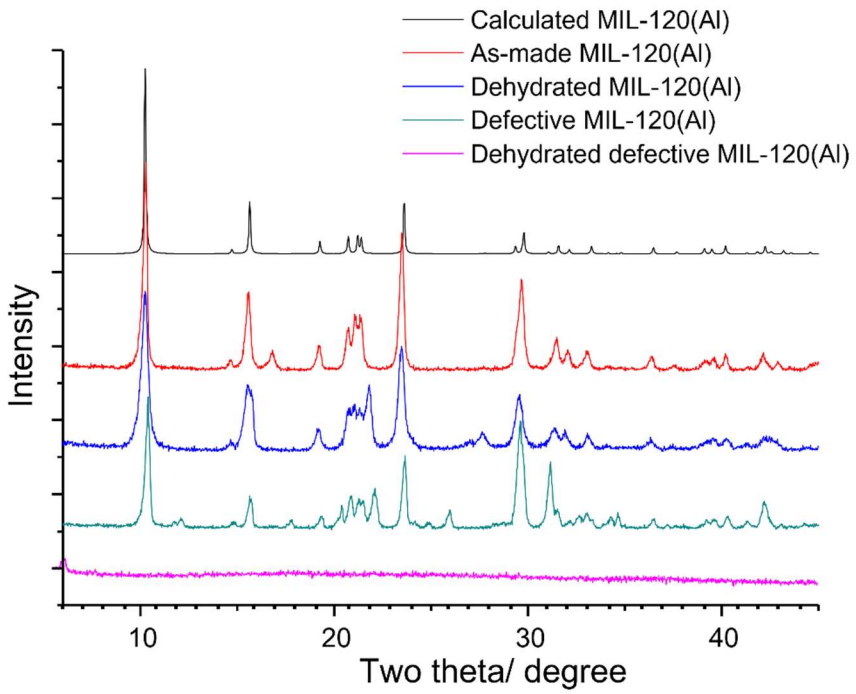

Figure S1. The PXRD patterns of parent MIL-120(Al) and defective MIL-120(Al) samples before and after dehydration.

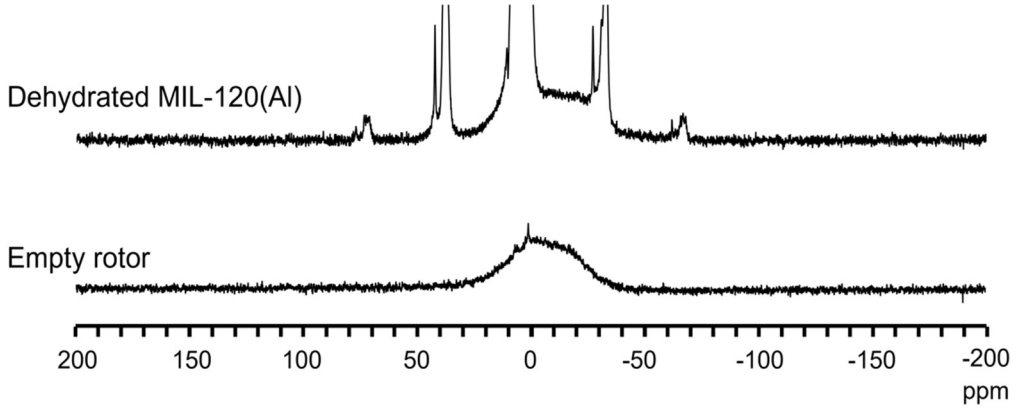

Figure S2. ^{1}H MAS NMR spectra of empty rotor (bottom) and dehydrated MIL-120(Al) acquired under the identical spectrometer conditions.

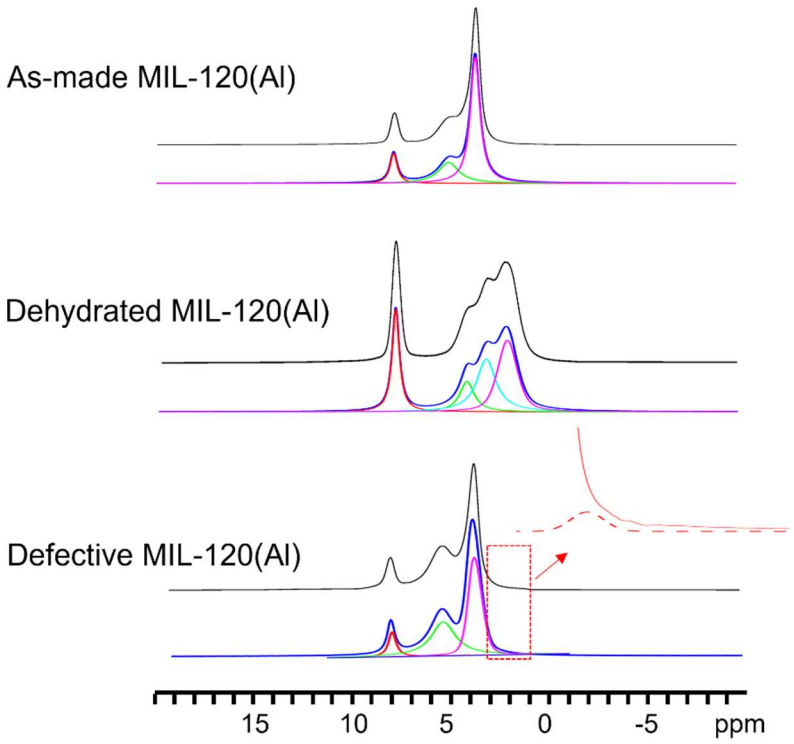

Figure S3. The deconvolution of ^{1}H MAS NMR spectra of as-made MIL-120(Al), dehydrated MIL-120(Al) and defective MIL-120(Al). The small signal in the inert is likely due to charge balancing OH^{-}.

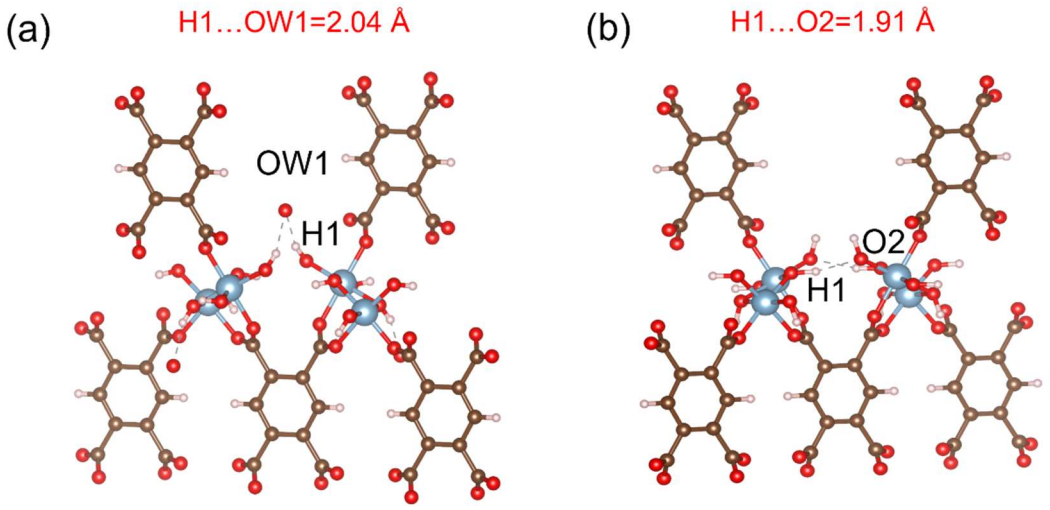

Figure S4. Illustration of hydrogen bonding in as-made MIL-120(Al) (structure from XRD) and dehydrated MIL-120(Al) (structure optimized by DFT calculation).

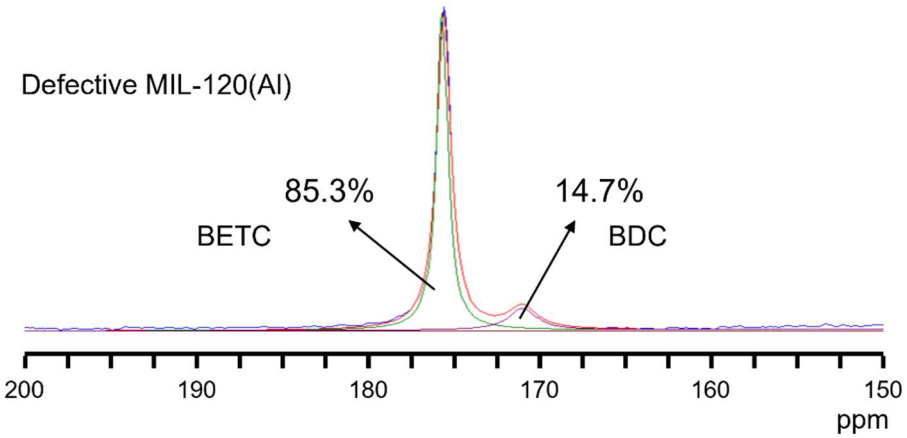

Figure S5. Deconvolution of $^{1}H \rightarrow {}^{13}C$ CP MAS NMR spectra of defective MIL-120(Al).

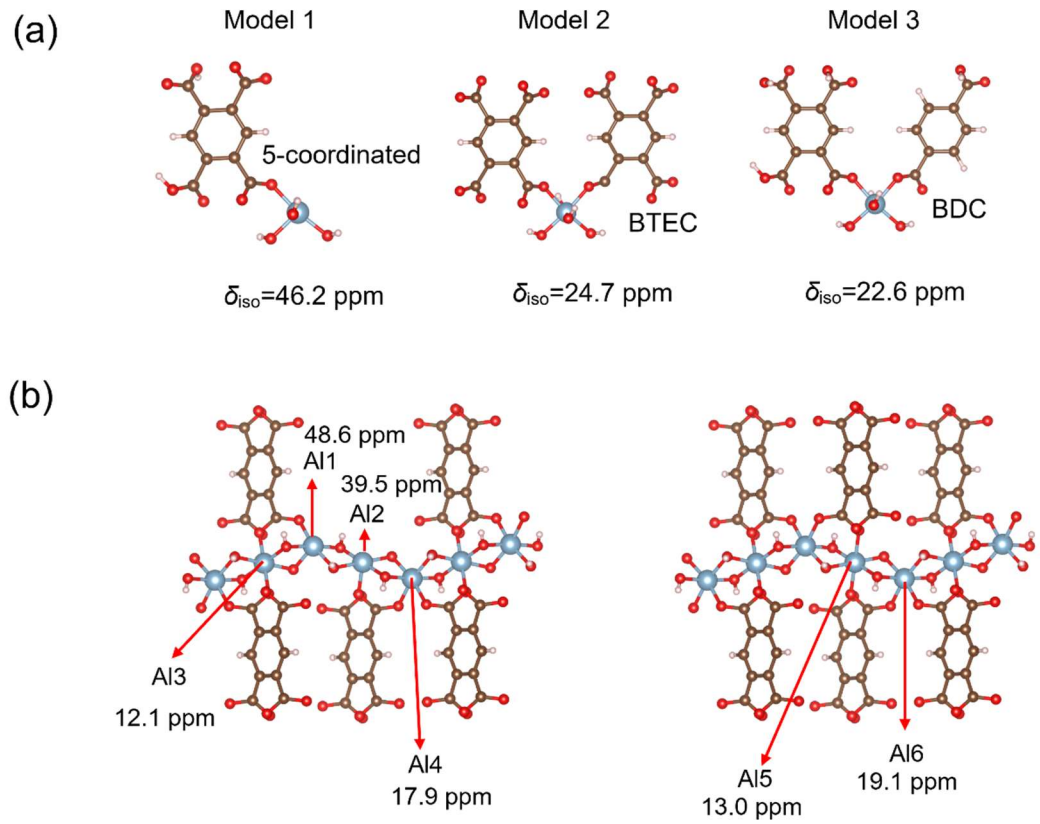

Figure S6. (a) Simple cluster models of representative local Al environments. Model 1: 5-coordinated Al; Model 2: defect free 6-coordinated Al with two BTEC linkers; Model 3: 6-coordinated Al bound to one BTEC and one BDC linkers. Note: the 5-coordinated Al has the largest chemical shift and the Al bout to one BTEC and one BDC has the smallest chemical shift. (b) A larger cluster model shows that the defect sites (5-coordinated Al1 and Al2) have the largest chemical shift. The 6-coordinated Al sites bound to two BTEC linkers, which are immediately adjacent to the defect sites, have chemical shifts smaller that the corresponding sites in defect-free region.

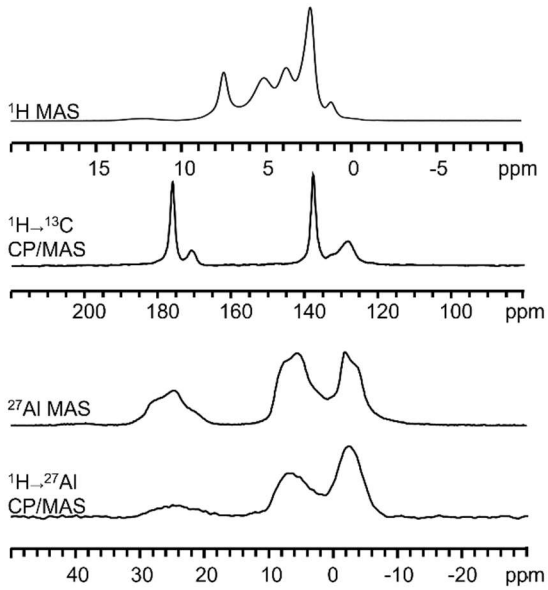

	δ_{iso}(ppm)	$\lvert C_Q \rvert$(MHz)	η_Q
Experiment (from 1DMAS)			
S4 (Site 4)	-0.40	4.5	0.20
S3 (Site 3)	9.6	8.8	0.34
S2 (Site 2)	10.0	5.4	0.35
S1 (Site 1)	29.5	6.1	0.70

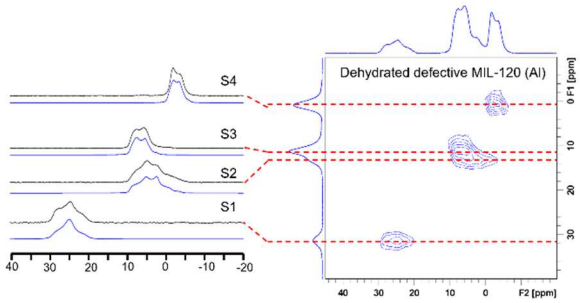

Figure S7. ^{1}H MAS, ^{1}H → ^{13}C CP MAS, ^{27}Al MAS, ^{1}H → ^{27}Al CP MAS, 3QMAS ^{27}Al NMR spectra of defective MIL-120(Al) after dehydration.

Table S1. Summary of Al…H distance of as-made MIL-120(Al) and dehydrated MIL-120(Al). The element labels are the same as the cif deposited in CCDC 789875.

Unit(Å)	As-made MIL-120(Al)	Dehydrated MIL-120(Al)
Al1…H1	2.372	2.428
Al1…H2	2.332	2.548
Al1… H3	4.367	4.337
Al2…H1	2.492	2.504
Al2…H2	2.429	2.441
Al2…H3	5.232	5.250